# Supplementary Information

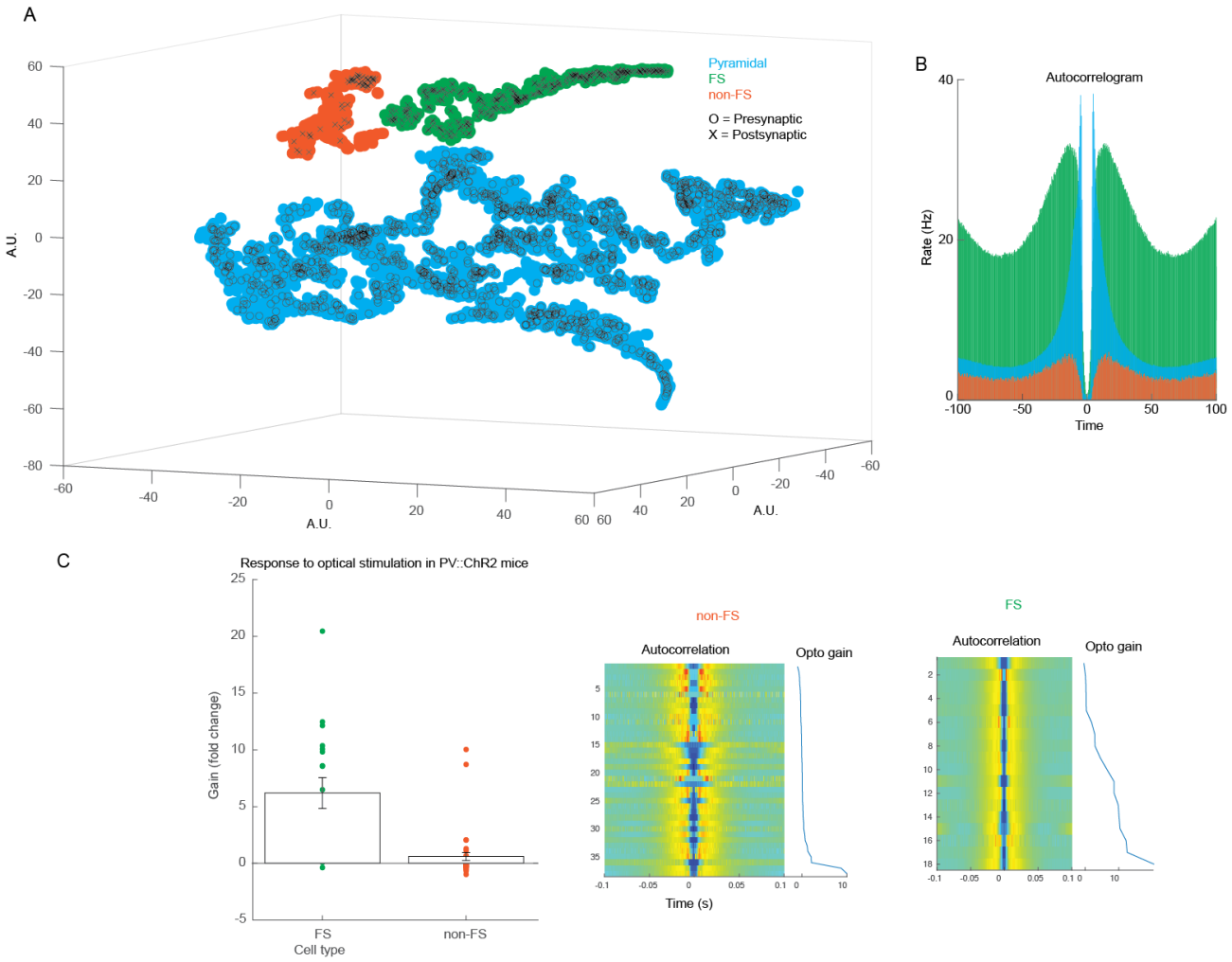


**Figure S1. Classification of cell types. Related to Figures 1-7.**

**A.** Three classes of neurons were identified using single cell physiological properties. Each neuron was defined by five features: mean rate, mode ISI, burstiness and spike asymmetry. For clustering analysis, these four dimensions were reduced to three using t-SNE and a density-based clustering algorithm was used on the three-dimensional space define the edges between clusters. Pyramidal neurons are shown in blue, fast spiking interneurons in green , and non-fast spiking

interneurons in orange. To confirm unit identity, we determined which neurons were mono-synaptically connected. Presynaptic pyramidal cells are shown with circles and postsynaptic interneurons cells with crosses. **B.** Average autocorrelation histograms for the three groups. **C.** Response of neurons classified as FS or non-FS to optical stimulation with 450 nm light in PV::ChR2 mice. **D.** For all cells in C, the autocorrelations outside of stimulation and the optical gain.

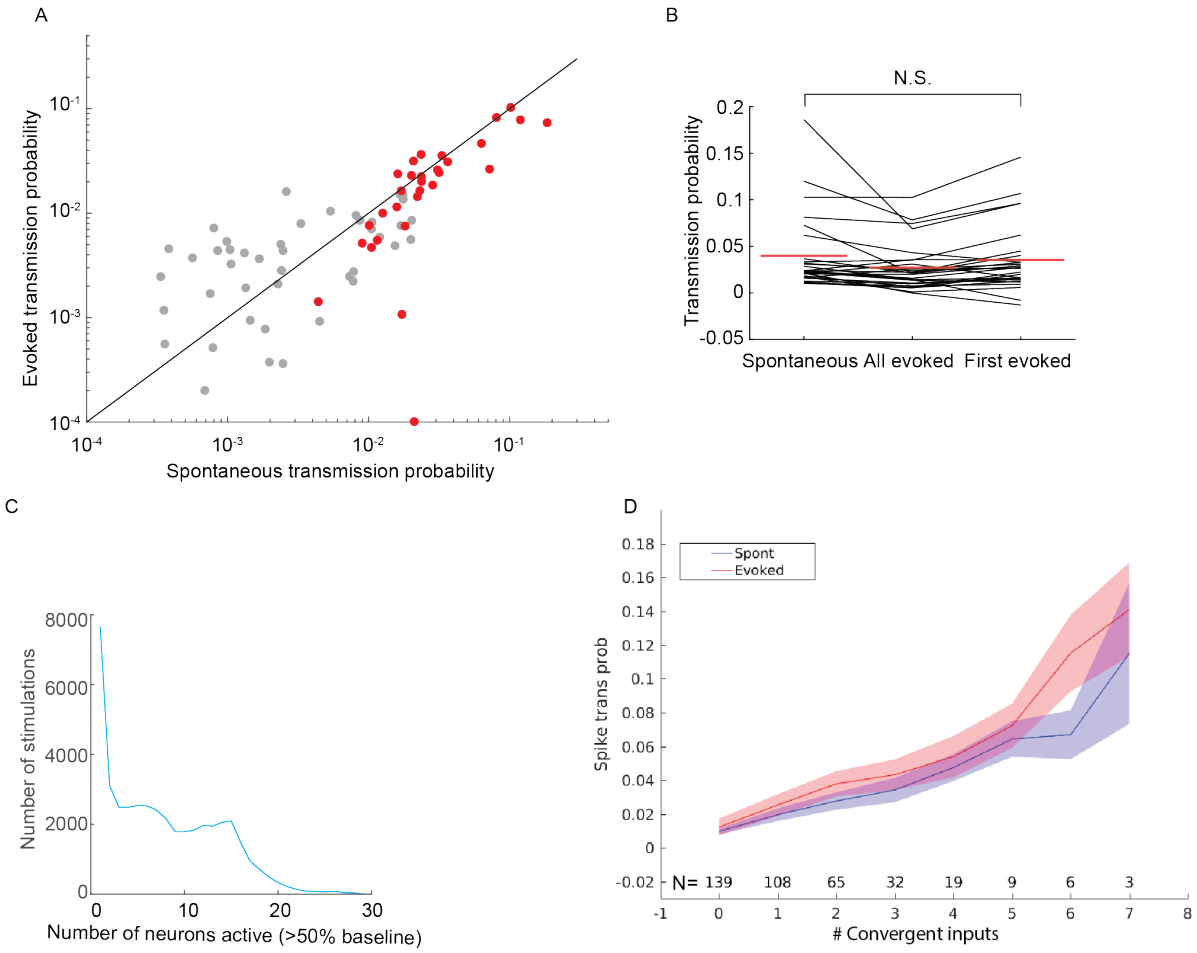


**Figure S2. Experiments related to classification of monosynaptic connections. Related to Figure 2.**

**A.** Transmission probability for spontaneous versus all juxtacellularly evoked spikes. **B.** Transmission probabilities for the 30 juxtacellular pairs for spontaneous spikes, all evoked spikes, or first evoked spike only. **C.** For all experiments with optogenetic stimulation of pyramidal neurons, the distribution of the number of neurons recruited per stimulus. **D.** The gain in transmission probabilities induced by increasing numbers of presynaptic cells spiking within a 2 ms window was not different for spontaneous versus optogenetically evoked spikes.

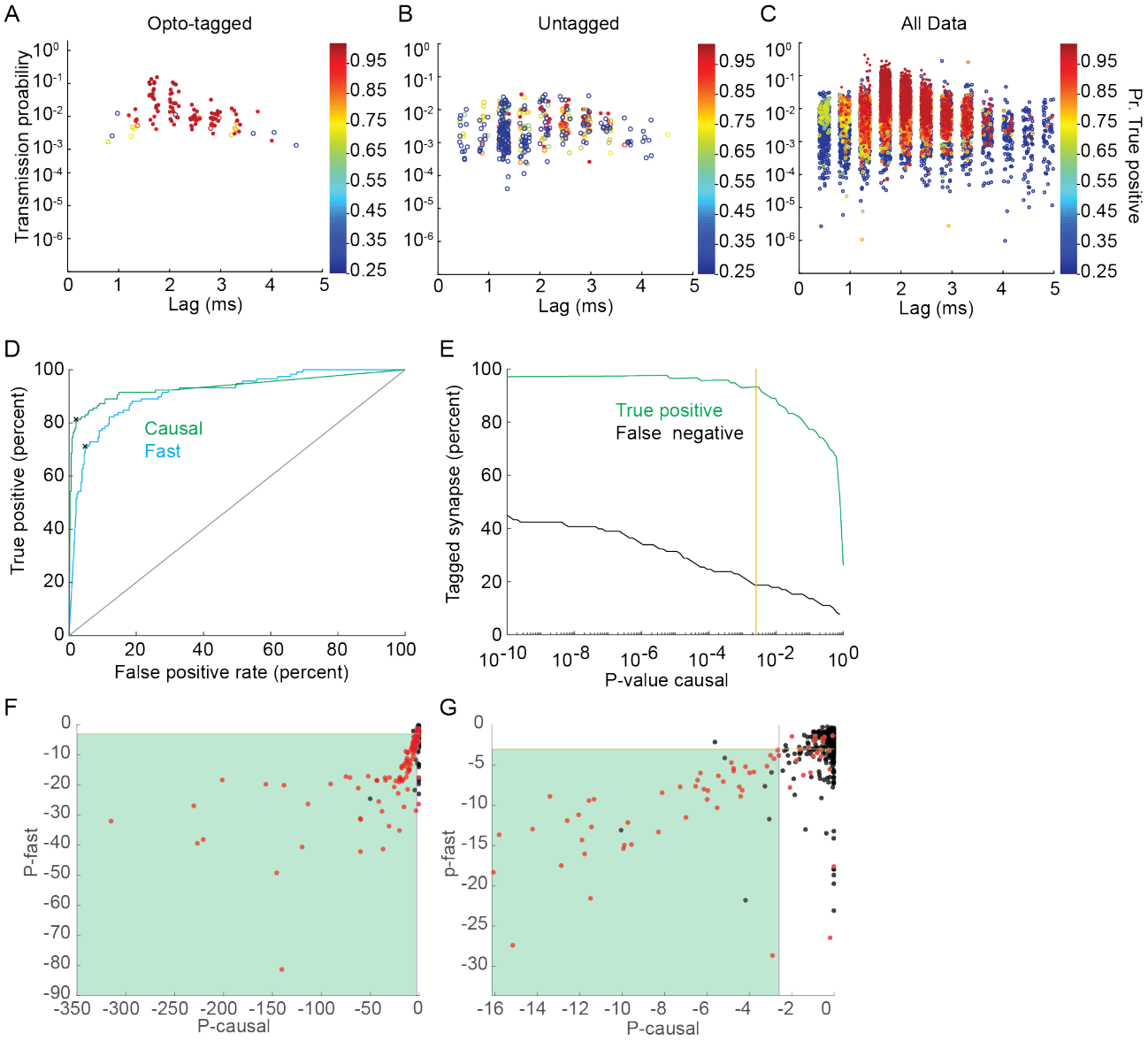

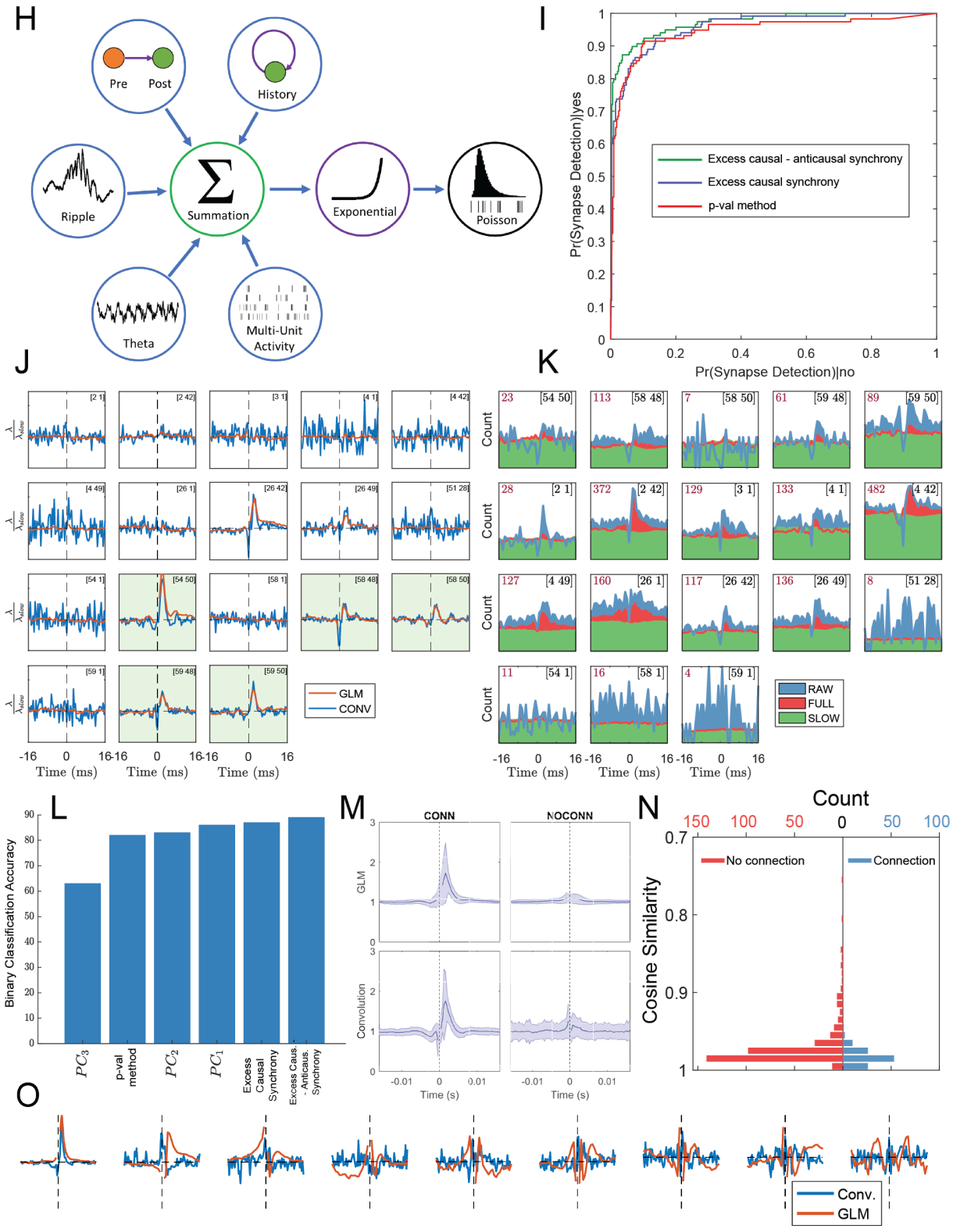


**Figure S3. Performance of detection methods. Related to Figure 2 and STAR Methods.**

**A.** Transmission probability as a function of time from the presynaptic spike (lag), with the p-value of being a monosynaptic connection plotted in color, for the CCGs tagged as monosynaptic connections. **B.** Same as in A, but for those pairs tagged as not being monosynaptic connections. **C.** Same as A, for the full population. **D.** Receiver operator characteristic curve using the $P_{Causal}$ and $P_{Fast}$ values ('Causal'), or just $P_{Fast}$ value ('Fast'). The black asterisks marks chosen threshold for classification. **E.** Hit (true positive) and miss (false negative) rates for the chosen p-values. **F.** Range of $P_{Causal}$ and $P_{Fast}$ corresponding to the chosen values for connection detection. Connections are in red, non-connections in black. **G.** Same as in G but zoomed in for clarity. **H.** Overview of GLM **I.** ROC figure comparing classification performance of three features (see Methods). The 'p-val' feature (equivalent to the ROC for the convolution method) performs similarly to summing the excess synchrony in the causal bins. Classification accuracy can be improved by taking the difference between the causal and anti-causal directions **J.** Visual comparison of GLM and convolution kernels show good agreement. Green background indicates connections **K.** Visualization of total modulation (Red+Green) accounted for by the GLM vs. the raw CCG (Blue), suggesting that there exists significant excess synchrony that could not be predicted by the Theta, Ripple, MUA and constant terms **L.** Separability of manually defined features and first three principal components from the corrected CCGs. Classification accuracy was defined as the mean binary loss from classification by a linear SVM. The single best predictor was the difference in causal and anti-causal synchrony (89%) **M.** Average connection and no-connection kernels for the GLM and convolution method. **N.** Histogram of cosine similarity scores between the CONV and GLM derived kernels for connected (Blue) and non-connected (Red) pairs. Mean cosine similarity for connected and unconnected pairs was 98.22% and 96.55% respectively **O.** First 9 principal components from GLM and convolution kernels.

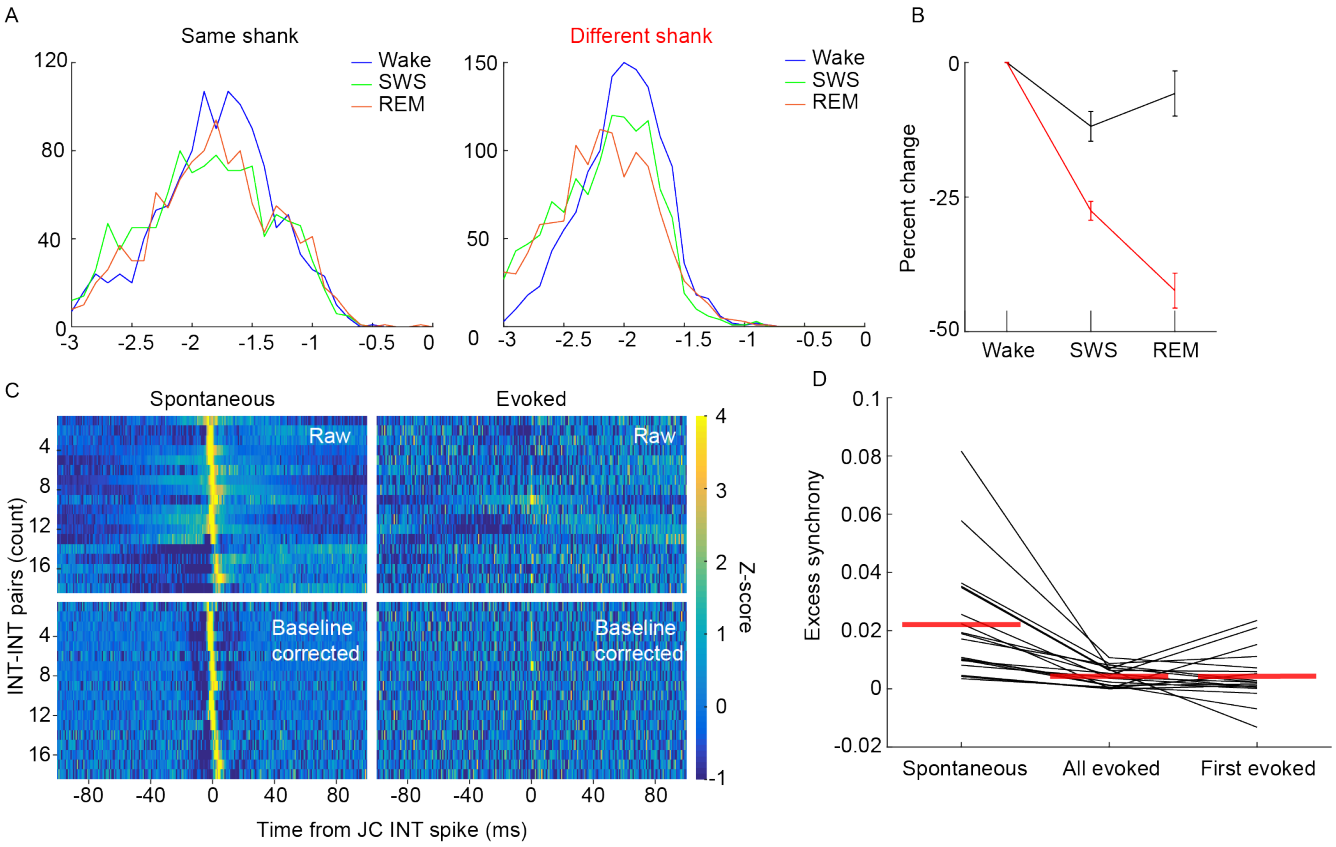


**Figure S4. State modulation or PYR-INT connections, and effect of juxtacellular stimulation of single interneurons on INT-INT synchrony. Related to Figure 3.**

**A.** PYR-INT transmission probability during waking (Wake), slow wave sleep (SWS) and rapid-eye movement sleep (REM), for neuron pairs recorded on the same shank (left) or different shanks (right). **B.** Transmission probabilities were lower during SWS and REM as compared to wake for both same shank and different shank pairs (same shank: wake vs SWS, signtest = $1.145^{-5}$, wake vs REM, signtest = 0.0165; different shank: wake vs SWS, signtest = $1.52^{-52}$, wake vs REM, signtest = $2.73^{-69}$). During SWS and REM the transmission probability was decreased more for different shank pairs as compared to same shank pairs (SWS, ranksum = $4.25^{-14}$; REM, ranksum = $2.52^{-38}$). **C.** CCGs for example interneuron pairs with one interneuron recorded with the silicon probe and one with the juxtacellular electrode. *Left:* CCG with only spontaneous

spikes from the juxtacellularly recorded cell. *Right:* CCG with only current-evoked spikes. **D.** Zero-lag synchrony is significantly lower for evoked versus spontaneous spikes (N =18 pairs, all evoked: $p=7.6^{-6}$, first evoked: $p=1.3^{-3}$).

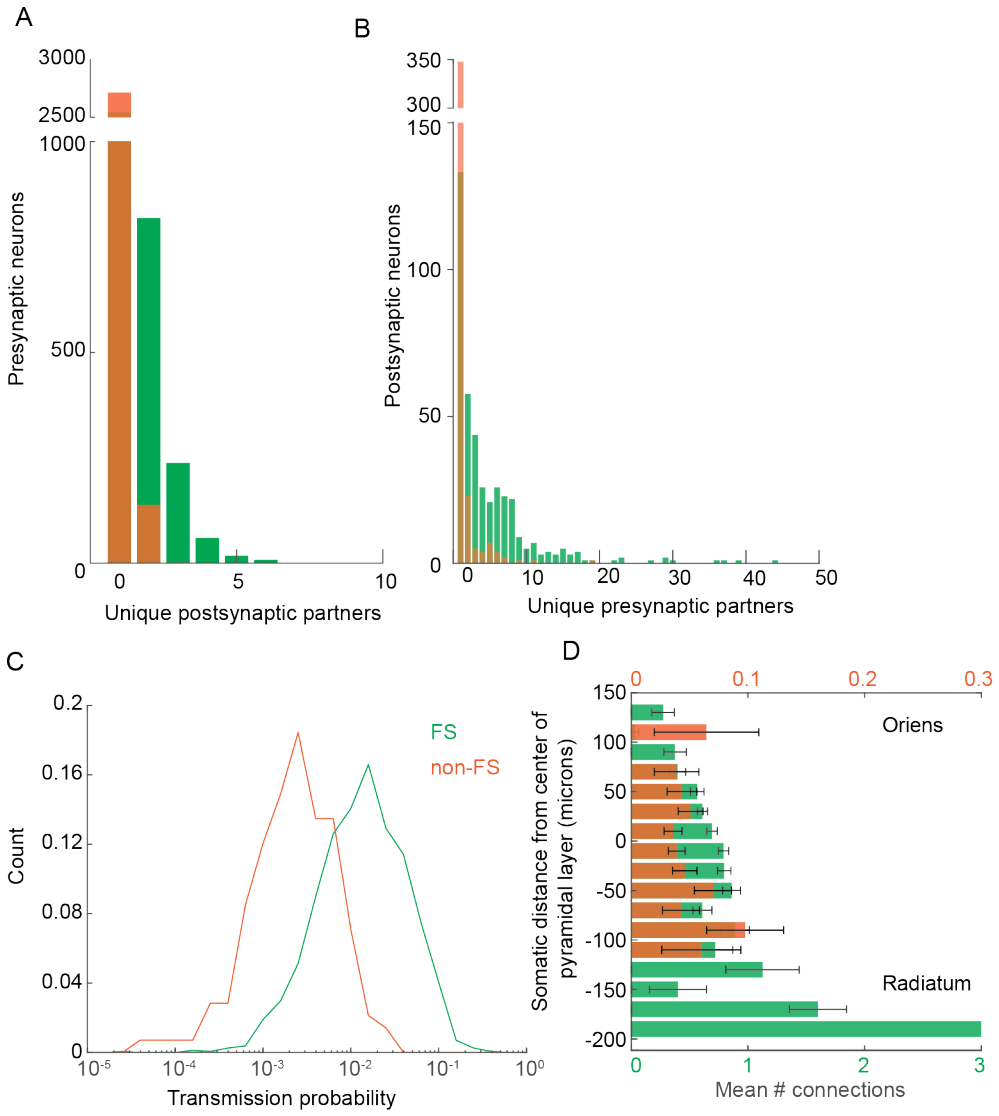


**Figure S5. Organization of connections by cell type. Related to Figure 4.**

**A.** Distribution of the number of unique postsynaptic neurons for both types across the population of presynaptic neurons. **B.** Distribution of the number of unique presynaptic neurons

for both types across the population of presynaptic neurons. **C.** Distribution of transmission probabilities for each interneuron type. **D.** Number of connections with each interneuron types for pyramidal neurons with different somatic locations. Pyramidal neurons at least 50 μm towards radiatum versus at least 50 μm towards oriens have more connections with FS interneurons ($p=4.0^{-4}$, N =1573 FS interneurons), but no difference in connectivity with non-FS ($p=0.33$ N =142).

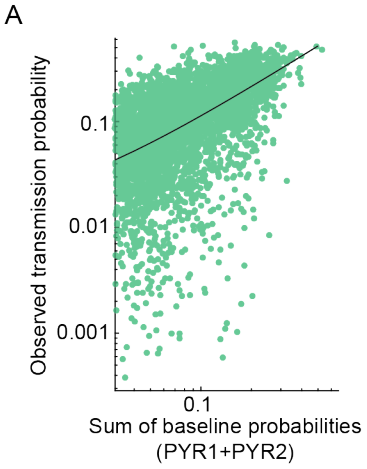


**Figure S6. Presynaptic cooperativity for all pairs. Related to Figure 5.**

**A.** Correlation of observed transmission probability (for the 0-0.4 ms PYR/PYR ISI condition) with the expected transmission probabilities based off of the linear sum of the two presynaptic neurons not conditioned on ISI.

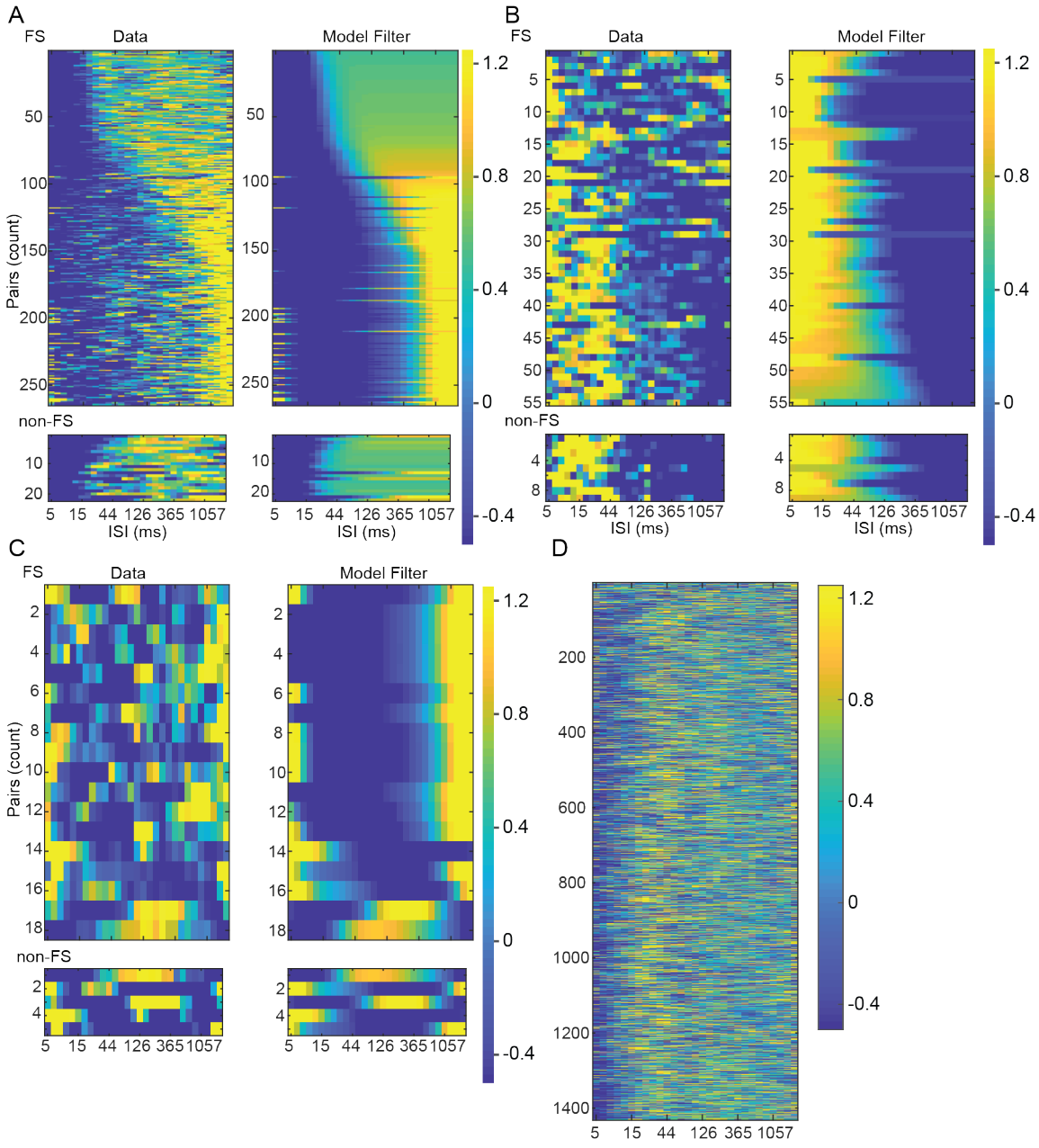


**Figure S7. Raw data and model fits for short-term synaptic dynamics. Related to Figure 6.** **A.** Connections in which depression alone was the most parsimonious fit on left, model fits on right. Data for FS cells on top, and non-FS cells on bottom. **B.** Same as A for pairs which facilitation alone was the most parsimonious fit. **C.** Same as in A for pairs in which the full model was the best fit. **D.** Pairs which were not well fit.